

Solar Cells

Colloidal Zeta Potential Modulation as a Handle to Control the Crystallization Kinetics of Tin Halide Perovskites for Photovoltaic Applications

Junfang Wang, Junjie Huang, Muhammad Abdel-Shakour, Tianhua Liu, Xu Wang, Yongle Pan, Lixia Wang, Enhao Cui, Jin-Song Hu,* Shihe Yang,* and Xiangyue Meng*

Abstract: Tin halide perovskites (THPs) have demonstrated exceptional potential for various applications owing to their low toxicity and excellent optoelectronic properties. However, the crystallization kinetics of THPs are less controllable than its lead counterpart because of the higher Lewis acidity of Sn^{2+} , leading to THP films with poor morphology and rampant defects. Here, a colloidal zeta potential modulation approach is developed to improve the crystallization kinetics of THP films inspired by the classical Derjaguin-Landau-Verwey-Overbeek (DLVO) theory. After adding 3-aminopyrrolidine dihydro iodate (APDI_2) in the precursor solution to change the zeta potential of the pristine colloids, the total interaction potential energy between colloidal particles with APDI_2 could be controllably reduced, resulting in a higher coagulation probability and a lower critical nuclei concentration. In situ laser light scattering measurements confirmed the increased nucleation rate of the THP colloids with APDI_2 . The resulting film with APDI_2 shows a pinhole-free morphology with fewer defects, achieving an impressive efficiency of 15.13 %.

Introduction

Hybrid organic–inorganic lead halide perovskites have emerged as a prominent contender for photovoltaic applications that can guarantee low-levelized cost-of-electricity.^[1] The power conversion efficiency (PCE) of the single-junction perovskite solar cells (PSCs) has achieved a certified value of 26.1 %.^[2–5] However, commercial expansion of lead-based PSCs may cause human health and environmental risks because of the hazardous lead.^[6–8] Tin halide perovskites are the most prospective substitute for lead-free perovskites due to their high charge carrier mobility ($1000 \text{ cm}^2 \text{ v}^{-1} \text{ s}^{-1}$),^[9] low exciton binding energies (~

18 meV),^[10] and long lifetime of hot carriers (more than 1 ns).^[11] Recently, tin halide perovskites have demonstrated exceptional achievements in various optoelectronic applications such as solar cells,^[12–22] field-effect transistors,^[23–25] light-emitting diodes,^[26–27] photodetectors,^[28] and lasers.^[29] The PCE of tin halide PSCs has exceeded 14 %, demonstrating the immense promise of tin halide perovskites for photovoltaic applications.^[30–35] However, the crystallization kinetics of THPs are less controllable because of the higher Lewis acidity of Sn^{2+} than Pb^{2+} , resulting in the unbalanced crystal nucleation and growth rate of tin halide perovskite films with poor morphology and abundant defects.^[36] Numerous attempts have been explored to control the crystallization kinetics of tin halide perovskite films to achieve fast nucleation and slow crystal growth.^[37–40] However, progress has been hampered by poor understanding of the relationship between the crucial colloidal chemistry of the perovskite precursor solution and the crystallization kinetics of perovskite films.

Perovskite precursor solution has been characterized as a colloidal dispersion in a mother solution, rather than a pure solution.^[41] The local chemical environment of the colloids in perovskite precursor solution plays a prominent role in the kinetics of perovskite film crystallization. Changing the organic–inorganic combination of the colloids in the precursor solution has been shown to affect the morphology, grain size, and crystallinity of perovskite films, as first reported by Yan et al.^[42] Furthermore, McMeekin et al. conducted an investigation into the effects of hydrohalic acids on the dissolution of the colloidal framework and the perovskite precursor solution. A superior perovskite film, in terms of grain size, crystallinity, and charge-carrier mobilities, was observed when the precursor solution's

[*] J. Wang, J. Huang, M. Abdel-Shakour, T. Liu, X. Wang, Y. Pan, L. Wang, E. Cui, X. Meng
School of Optoelectronics, Center of Materials Science and Optoelectronics Engineering, University of Chinese Academy of Sciences, Beijing, 100049, China
E-mail: mengxiangyue@ucas.ac.cn

J.-S. Hu
Beijing National Laboratory for Molecular Sciences. CAS Key Laboratory of Molecular Nanostructure and Nanotechnology, Institute of Chemistry, Chinese Academy of Sciences, Beijing, 100190, China
E-mail: hujs@iccas.ac.cn

S. Yang
Guangdong Key Lab of Nano-Micro Material Research, School of Advanced Materials, Shenzhen Graduate School, Peking University, Shenzhen, 518055, China
E-mail: yangsh@pkusz.edu.cn

M. Abdel-Shakour
Chemistry Department, Faculty of Science, Assiut University, Assiut 71516, Egypt

colloidal size distribution was optimized.^[43] Kim et al. reported that a reduction in colloid size after adding iodide ions into the precursor solution could produce perovskite films with far better crystallinity and fewer defects.^[44] Previous studies have investigated deeply the colloidal composition and size distribution of perovskite colloids.^[45–46] However, the effects of zeta potential (φ_d) of the colloids in the perovskite precursor solution have not been investigated in depth, and the relationship between the colloidal zeta potential and the nucleation process of perovskite colloids remains to be understood.

In this work, for the first time, the relationship between the colloidal zeta potential and the nucleation rate of tin halide perovskite films is established. It is shown that adding a small amount of 3-aminopyrrolidine dihydroiodate (APDI₂) to the pristine perovskite precursor solution can considerably change the zeta potential of pristine perovskite colloids, due to the adsorption of APD²⁺ in the stern layer of the perovskite colloids. In situ laser light scattering spectroscopy revealed that the perovskite colloids of added APDI₂ with lower absolute zeta potential accelerated the nucleation process of perovskites, which was ascribed to the reduction of total interaction potential energy (E_p) between colloidal particles and reduced critical concentration for nucleation (c_{\min}). The fast nucleation rate during the film formation produced the APDI₂ perovskite film with pin-hole-free morphology, excellent crystallinity, and fewer defects compared to the pristine tin halide perovskite film. Consequently, the PCE of the PSCs with APDI₂ rocketed to over 15%, which is one of the highest PCE for tin halide PSCs to date. This study shows how the colloidal zeta potential property of perovskite precursor solutions influences the photovoltaic performance of tin halide PSCs, providing guidelines for the precise control of the nucleation dynamics in tin halide perovskite films for promoting the photovoltaic performance.

Results and Discussion

The THP precursor solution has been noticed to exhibit characteristics of a colloidal dispersion rather than a homogeneous pure solution.^[47] THP film crystallization kinetics are highly dependent on the precise chemical condition of colloids in the THP precursor solution.^[48–50] According to the classical Stern model, the interaction between charged colloidal particles is mediated by their electric double layers (the inner stern layer and the outer diffuse layer).^[51–53] Zeta potential (φ_d) is the electrical potential in the interfacial electric double layer at the location of the slipping plane (Figure S1), which measures the magnitude of electrostatic repulsion/attraction interaction between particles.^[54] As proposed by the classical Stern model theory,^[55] zeta potential is one of the fundamental parameters that can be used to modulate the nucleation kinetics of colloidal particles. If the colloidal particles have a large negative or positive zeta potential, they will tend to repel each other. However, if the colloidal particles have low absolute zeta potential values, then there is reduced

force to prevent the colloidal particles from coming together and nucleating. We set out to investigate the effects of zeta potential on the colloidal nucleation kinetics.

Firstly, we measured zeta potential of the THP precursor solution (Figure S2). As shown in Figure 1a, after introducing 2 mol% APDI₂ in the pristine perovskite precursor solution (81 mol% FAI, 15 mol% SnF₂, 15 mol% PEABr, 100 mol% SnI₂, 2 mol% APDI₂), the zeta potential of perovskite colloidal particles was dramatically changed from -4.22 mV to 0.69 mV (Table S1). Plausibly, the zeta potential change can be ascribed to the strong chemisorption of the multivalent cations (APD²⁺) into the Stern layer of the colloids.^[52] The electric double-layer structure of the THP colloids with and without APDI₂ can thus be deduced as schematically illustrated in Figure 1b. On the basis of the negative zeta potential value and the photoluminescence signal for the SnI₆⁴⁻ in the pristine perovskite precursor solution (Figure S3), the colloidal nucleus is primarily composed of the FASnI₃ perovskite structure and the large SnI₆⁴⁻ anions (Figure S4). In the Stern layer, FA⁺ is strongly bonded to the colloidal nucleus. The diffuse layer is located at the outer edge of the total colloidal particle, where FA⁺ is loosely attached (Figure S5). As such, the initial colloidal particles should have a negative zeta potential (-4.22 mV). As shown in Figures 1b and S1, due to the strong interaction between APD²⁺ and SnI₆⁴⁻ at the stern layer, the zeta potential of the colloid with APDI₂ is expected to increase to the positive value (0.69 mV). Nuclear magnetic resonance (¹H NMR) spectroscopy and Fourier transform infrared (FTIR) spectroscopy were also conducted to confirm the strong interaction between APD²⁺ and SnI₆⁴⁻. From the ¹H NMR spectra as shown in **Figures 1c and Figure S6**, the two peaks of APDI₂ at 7.97 and 8.69 ppm were obviously shifted to the value of 8.24 ppm, and a slightly down-field shift for the protons in -CH₂- close to the -NH₂⁺ and -NH₃⁺ cation was observed after adding SnI₂ in the APDI₂ solution, indicating the strong chemical interaction between APD²⁺ and SnI₆⁴⁻. Furthermore, the FTIR spectroscopy depicted in Figure S7 shows a shift to lower wavenumbers for the N–H and –NH₂– stretching vibration peaks of the APDI₂ at 3088 cm⁻¹ and 3434 cm⁻¹. This shift can be attributed to the deformation of the electron cloud and reduced bond stiffness induced by the interaction between APDI₂ and SnI₆⁴⁻.

To investigate the relationship between the nucleation process and zeta potential of THP colloids, we resort to the classical Derjaguin-Landau-Verwey-Overbeek (DLVO) theory.^[56] The total interaction potential energy (E_p) of two colloid particles to coagulate for nucleation is the sum of their van der Waals interaction energy (E_{cdw}) and the electric repulsive interaction energy (E_{es}).^[57–58] The latter can be calculated from equation 1 below:

$$E_{\text{es}} = 2\pi\epsilon a\varphi_d^2 \exp[-\kappa h] \quad (1)$$

where κ is the inverse Debye screening length of the diffuse layer around the spherical particles in the solution, h is the separation distance between particle surfaces, a is the radius of particles, φ_d is the zeta potential, ϵ is the permittivity of

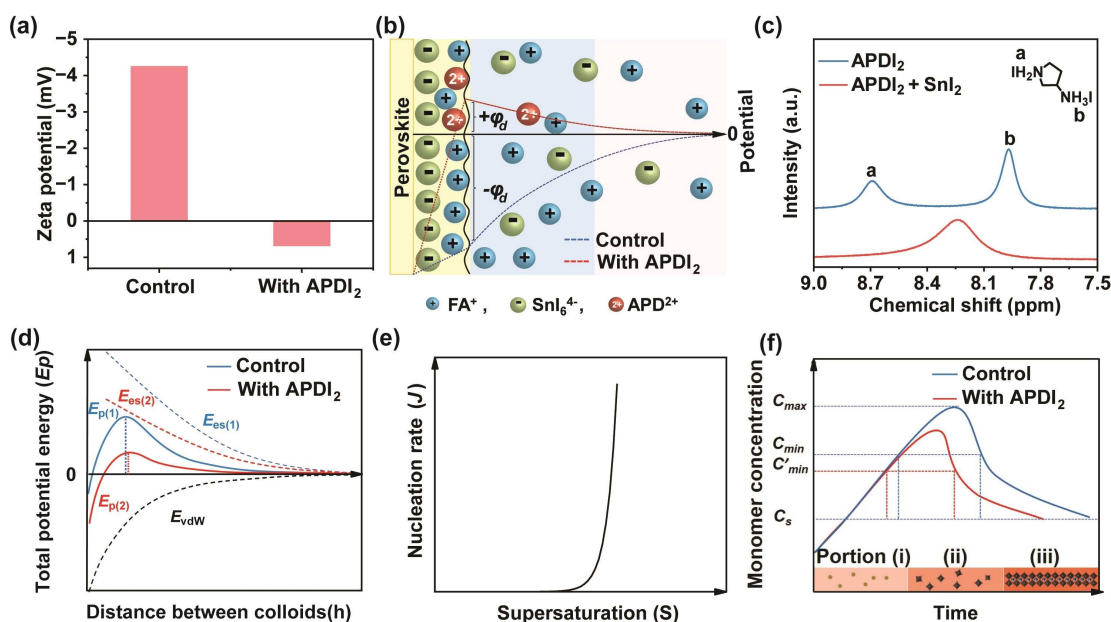


Figure 1. Zeta potentials of precursor solutions and their effects on the colloidal potential energy surfaces and nucleation kinetics. (a) Zeta potentials of precursor solutions with and without APDI₂. (b) Schematic of the electric double layer structure according to Stern's theory and the corresponding zeta potential (φ_d) in perovskite precursor solutions with and without APDI₂. (c) ¹H NMR spectra of APDI₂ and APDI₂-SnI₂ in DMSO-*d*₆ solutions. (d) The influence of zeta potential on the total interaction potential energy of the tin halide perovskite colloidal particles with and without APDI₂. (e) Plot of the nucleation rate versus the supersaturation. (f) The LaMer diagram of nucleation and growth kinetics for perovskite films with and without APDI₂.

the dispersion medium. As shown in Figure S8, the colloidal size (a) of the THP precursor solution with APDI₂ showed a negligible change after adding APDI₂. According to equation 1, the lower the square of zeta potential (φ_d^2) of APDI₂ colloids, the lower E_{es} , resulting in a lower E_p (Figure 1d). This leads to a higher coagulation probability, thus facilitating the nucleation of the interacting APDI₂ colloidal particles.

According to DLVO theory, the critical concentration of coagulation for nucleation (c_{min}) is expressed in equation (2) in terms of zeta potential of the colloidal particles:

$$c_{min} = 1.86 \times 10^6 \left(\frac{A}{kT} \right)^2 \frac{1}{z^2 \varphi_d^4} \quad (2)$$

where A is the Hamaker constant, T is the absolute temperature, k is Debye-Huckel parameter, z is charges of the counter-ion, φ_d is zeta potential, respectively. It stands to reason that a decrease in four powers of zeta potential (φ_d^4) during the nucleation process of the FASnI₃-APDI₂ perovskite films will drastically reduce the critical concentration of coagulation for nucleation (c_{min}), and thus significantly increase the supersaturation degree ($S = (c - c_{min})/c_{min}$, c is perovskite precursor solution concentration). The increased supersaturation in the precursor solution with APDI₂, in turn, will decrease the total free energy of nuclei formation (equation S5 and Figure S9) and increase the nucleation rate (J_n) as given in Figure 1e and equation 3.

$$J_n = D \exp(-B(LnS)^{-2}) \quad (3)$$

where J_n is nucleation rate, and B is dominated by the interfacial energy between the colloidal crystals and the solution. As shown in Figure 1e, at first, the nucleation rate increases slowly as the supersaturation degree increasing under the condition of low saturation. However, after passing a certain threshold of supersaturation degree (controlled by parameter B in equation 3), the nucleation rate starts to rise exponentially with the supersaturation degree, and finally tends to an extreme value of the nucleation rate (controlled by parameter D).^[59] Therefore, the APDI₂ additives in THP precursor solution can considerably increase the supersaturation degree and enhance the nucleation rate.

As shown in Figure 1f, the LaMer graph is used to depict the overall nucleation and crystal growth processes of tin halide perovskite films and establishes the relation between the supersaturation degree of solution and the crystallization process. The concentration of monomers versus time can be divided into three portions: (i) colloids, (ii) nucleation, and (iii) crystal growth. When the monomer concentration reaches the critical nucleation concentration (c_{min}), the colloids will undergo a burst nucleation.^[60] Nucleation is terminated when the monomers concentration is lower than c_{min} . Given the above-presented results, the perovskite colloidal particles with APDI₂ have a lower absolute zeta potential and thus a lower value of c_{min} , ultimately driving up the nucleation rate and shortening the nucleation time.

Since the formation of perovskite nucleus at the initial stage of crystal nucleation can be probed by light scattering measurements to understand the nucleation mechanism,^[61–63] we tracked the light scattering intensity profiles of the perovskite films with and without APDI₂ during spin-coating by in situ laser light scattering (LLS) spectroscopy (Figure S10). From the two-dimensional maps of in situ LLS spectra (Figures 2a and 2b), after the antisolvent was dripped at 52 s, the perovskite film with APDI₂ exhibited much higher light scattering intensities most of the time during spin-coating. To get deep details about the nucleation rate, we plotted the scattering intensity at 450 nm across the spin coating time (Figure 2c). For the pristine tin halide perovskite film, the scattering intensity reached to the saturation intensity in a time span of 8.0 seconds (52.0–60.0 s). In contrast, the scattering intensity of the perovskite film with APDI₂ increased much faster, that is, within a much shorter time (2.0 seconds, 52.0–54.0 s), indicating a rapid nucleation rate for the perovskites after adding APDI₂. Besides, as APDI₂ is increased from 2% to 3%, the nucleation rate slows down, which is consistent with our zeta potential measurement (Figure S11). To directly see the evolution of nucleation rate, the first derivative of LLS spectroscopy intensity was also calculated (Figure 2d). The highest nucleation rate for the FASnI₃-APDI₂ perovskite was 3954 s⁻¹ within a very short time interval (0.5 s), which is to be compared with the much lower peak nucleation rate for the pristine FASnI₃ perovskite (1090 s⁻¹). On the other hand, in situ photoluminescence spectra showed that the addition of APDI₂ did not change the film growth kinetics (Figure S12). These results proved that the APDI₂ additives can drastically increase the bursting nucleation rate of tin halide perovskite films.

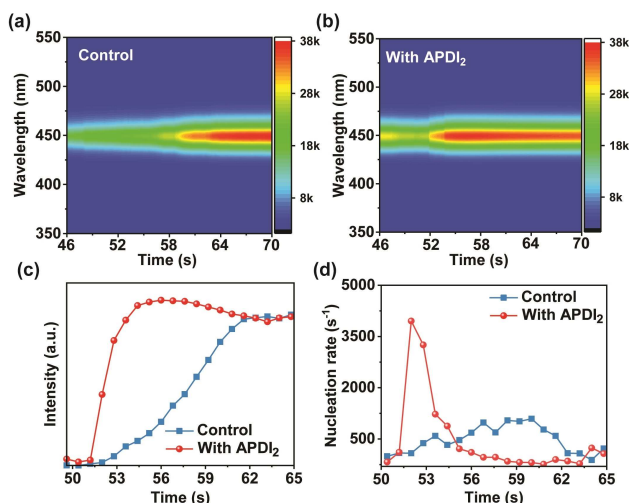


Figure 2. In situ laser light scattering spectroscopic investigation of the colloidal nucleation kinetics. In situ laser light scattering spectra as a function of spin coating time of the perovskite films (a) without and (b) with APDI₂. (c) Laser light scattering intensity evolution and (d) the nucleation rate calculated by the first derivative from the laser light scattering intensity evolution at the incident wavelength of 450 nm during spin coating.

Next, scanning electron microscopy (SEM) was performed to investigate the impact of nucleation rate on the quasi-2D perovskite film morphology by monitoring the transformation course from the colloid to perovskite films. As presented in Figure 3a, the pristine tin halide perovskite film was formed with many pin-holes and voids. In contrast, the film with APDI₂ was dense and fully covered by polycrystalline perovskites (Figure 3b). The improved quality of perovskite films with added APDI₂ suggested that faster nucleation rate encouraged homogeneous nucleation with more compact nucleation sites. Figure 3c showed the X-ray diffraction (XRD) spectra of the perovskite films with and without APDI₂. The films containing APDI₂ exhibited higher intensity with reduced full-width-at-half-maximum (FWHM) from 0.100 to 0.075 compared to the pristine FASnI₃ film (Figure S13), indicating the superior crystallinity of the perovskite film after adding APDI₂. The grazing-incidence wide-angle X-ray scattering (GIWAXS) pattern of the perovskite films with and without APDI₂ also confirmed the improved crystallinity for the perovskite film modified by APDI₂ (Figure S14). We calculated the residual strain of the perovskite films by using Williamson-Hall plots (Figure S15 and Equation S4).^[64] As indicated in Figure 3d, the tensile strain of the tin halide films with APDI₂ was also released.

To understand effects of nucleation rate on charge-carrier dynamics of the perovskite films, steady photoluminescence (PL) and time-resolved photoluminescence (TRPL) spectroscopies were conducted. As shown in Figure 3e, the perovskite film modified by APDI₂ showed stronger PL intensity, indicating a suppressed recombination. **Moreover, TRPL characterizations showed a prolonged PL lifetime of 24.7 ns for the perovskite film with APDI₂ (Figure 3f), which was much longer than that of the pristine tin halide perovskite film (14.1 ns).** The PL, TRPL, and SEM results with the range addition of APDI₂ from 1 mol% to 3 mol% revealed that the most pronounced composition of APDI₂ was 2 mol% (Figures S16, S17 and S18). The enhanced PL intensity and extended PL lifetime of films with APDI₂ can be ascribed to the reduced trap density, confirming that the fast nucleation rate induced by the precursor colloid containing APDI₂ with low absolute zeta potential was beneficial to improving the quality of perovskite film.

To investigate the trap densities in both perovskite films with and without APDI₂, space charge limiting current (SCLC) of hole-only devices was measured with the structure of ITO/PEDOT:PSS/perovskite/MoO₃/Ag (Figure 3g). The trap density (N_t) was determined by equation S6. As shown in Figure 3g, the hole trap density of pristine tin halide perovskite films without APDI₂ was $2.1 \times 10^{16} \text{ cm}^{-3}$. On the other hand, the hole trap density was decreased to $1.1 \times 10^{16} \text{ cm}^{-3}$ for the perovskite film with APDI₂, which was significantly lower than pristine perovskite film. According to these outcomes, trap states in perovskite films with APDI₂ can be successfully diminished thanks to their rapid nucleation rate.

Finally, we fabricated PSCs using the optimized THP precursor solution with low absolute zeta potential colloids.

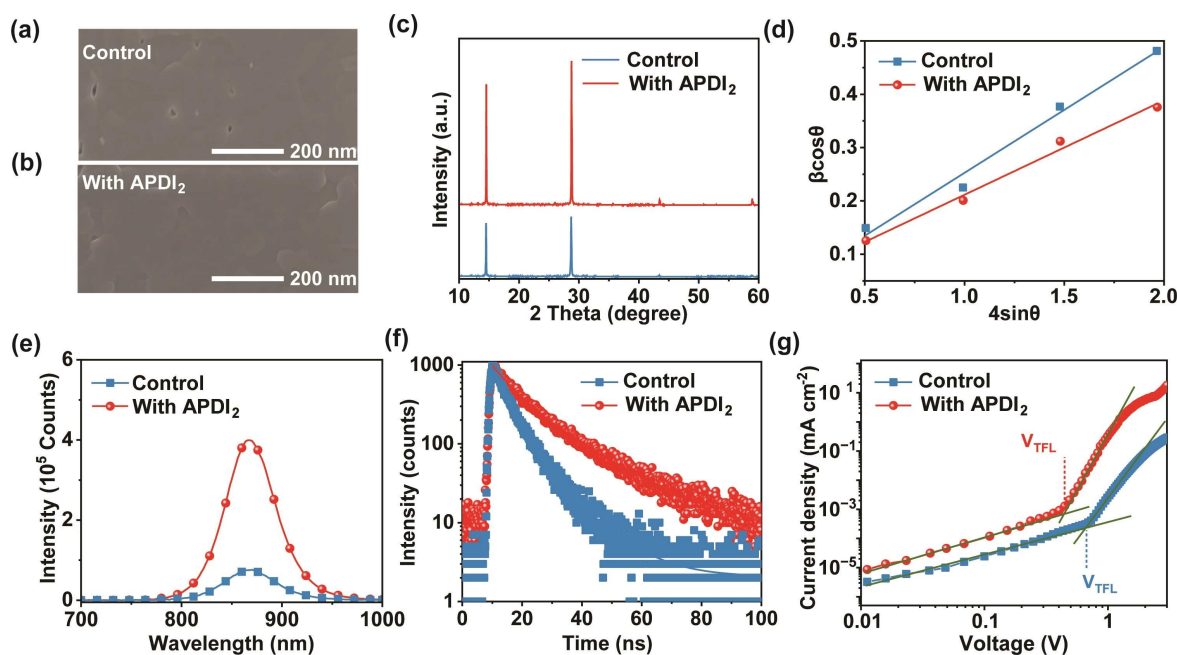


Figure 3. Effect of APDI₂ on the crystalline quality and optoelectronic properties of the perovskite films. Scanning electron microscope images of the perovskite films (a) without and (b) with APDI₂. (c) X-ray diffraction patterns of perovskite films with and without APDI₂. (d) Williamson–Hall plots fitting of the perovskite films with and without APDI₂. (e) Steady-state photoluminescence spectra and (f) time-resolved photoluminescence decay spectra for the perovskite films with and without APDI₂. (g) Dark J - V curves of the hole-only devices based on the perovskite films with and without APDI₂.

The inverted planar p-i-n with the structure of ITO/PEDOT:PSS/perovskite/NCBA/BCP/Ag was fabricated (Figure 4a). Since NCBA has a more favorable energy-level alignment, it was selected as the electron transport layer.^[65–66] Figure 4b showed the current density–voltage (J - V) curves of the champion PSC devices based on the control and APDI₂-containing films under simulated solar illumination (AM 1.5G and 100 mW cm⁻²). The fabricated PSCs based on the pristine tin halide perovskite film exhibited a champion PCE of 13.10% under the reverse scan. Significantly, the PSCs based on films modified by APDI₂, which processed from faster nucleation rate, produced a PCE of 15.13% under the reverse scan (Figure 4b) with an open-circuit voltage (V_{oc}) as high as 0.97 V, a short-circuit current density (J_{sc}) of 21.58 mA cm⁻² and a fill factor (FF) of 72.29% (Figure S19, Table S2). Impressively, a certified PCE of 14.81% was obtained for the PSCs with APDI₂ added (Figure S20). The enhancement of PCE was originated from significantly increased V_{oc} from 0.86 V to 0.97 V (Table S3), which resulted in a stable output power of 14.88% (Figure S21). Transient photovoltage measurements for the PSCs were performed to explain the reason for the enhancement in PCE. As depicted in Figure 4c, the PSCs based on the films with APDI₂ showed the charge recombination time constant of 79.98 μs, which was approximately ten times higher than that of the control device (8.06 μs). These results indicated that the recombination of photo-generated carriers in the perovskite film with APDI₂ was relatively low, which was beneficial for the improvement of V_{oc} in the devices.

Mott–Schottky curves were also measured to further study the cause of the V_{oc} enhancement (Figure S22). The built-in voltage (V_{bi}) of device based the perovskite film with APDI₂ (0.88 V) is considerably higher than of the control device (0.79 V), resulting in a better electron-hole separation collection for APDI₂-containing device. Furthermore, ideality factor measurement shows that the lower slope value of 1.71 kT/q in devices based on the perovskite film with APDI₂ than that in control devices (1.82 kT/q), suggesting the reduction of trap-assisted recombination in APDI₂-containing devices (Figure S23). Ultraviolet photoelectron spectroscopy and UV/Vis absorbance spectroscopy showed that valence band and conduction band for perovskite films modified by APDI₂ exhibited no change compared to the pristine tin halide perovskite films (Figures S24 and S25). To ensure the accuracy of the obtained J_{sc} , the incident photon-to-electron conversion efficiency (IPCE) spectra of the fabricated tin halide PSCs was measured (Figure S22). The integrated J_{sc} estimated from the IPCE curves were 21.23 and 21.67 mA cm⁻² for control and APDI₂-containing PSCs, respectively, which are close to the J_{sc} values obtained from the J - V curves (Figure S26). Importantly, the devices based on tin halide film with APDI₂ showed a high level of reproducibility (Figure S27) and superior stability after being stored in either the nitrogen-filled glovebox or in air (Figures S28 and S29).

To explore the charge transport process of the fabricated devices, dark J - V measurement was conducted. As shown in Figure 4d, the PSCs based on the film with APDI₂ exhibited lower dark current density (6×10^{-8} mA cm⁻²) than that in

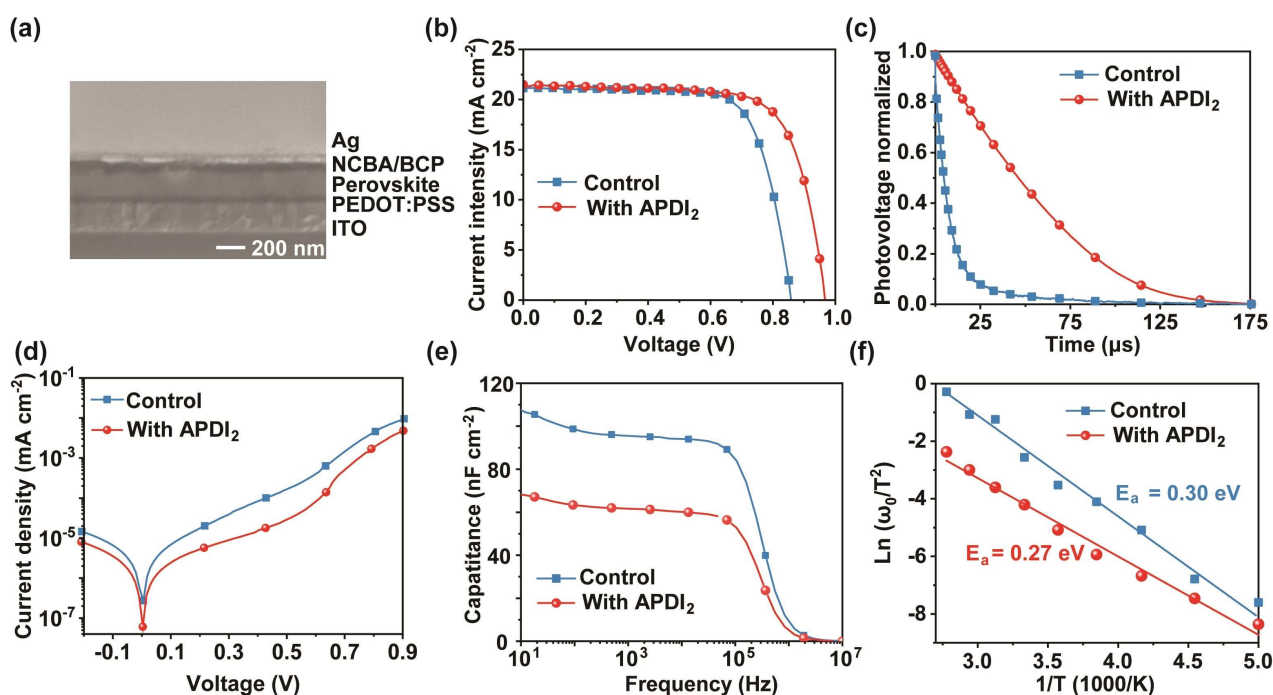


Figure 4. Effect of APDI₂ on the device performance. (a) Cross-sectional view scanning electron microscope image of the device based on the film with APDI₂. (b) *J*–*V* curves of the champion devices and (c) transient photovoltage decay profiles based on the films with and without APDI₂. (d) Dark *J*–*V* curves and (e) admittance spectra for devices based on based on the films with and without APDI₂ at 300 K. (f) The defect activation energy (E_a) from temperature-dependent admittance spectra for devices based on the tin halide perovskite films with and without APDI₂.

the control device ($2 \times 10^{-7} \text{ mA cm}^{-2}$). This decrease in dark current values indicated reduced charge recombination, which could be ascribed to lower defects in the film modified by APDI₂. To further elucidate the trap-state distributions affected by the faster nucleation rate induced by the APDI₂-containing precursor colloidal solution, the trap-state profiles have been investigated by using thermal admittance spectroscopy. The capacitance versus frequency (*C*–*f*) curves showed that the capacitance of device based on the perovskite films with APDI₂ exhibited a significantly reduction compared to that of the control device (Figure 4e), suggesting the decreased defect density in the film with APDI₂. We also acquired temperature-dependent *C*–*f* plots from 280 K to 320 K to probe the energy depth and the trap density of trap states (Figures S30 and S31). Evidently, the PSCs based on the tin halide perovskite films with APDI₂ exhibited a much lower density of trap state at energies between 0.25 and 0.45 eV than that of the control PSCs. By plotting $\ln(\omega_0/T^2)$ vs. $1/T$, the slope gives the trap state energy level (Figure 4f). The devices based on the perovskite film with APDI₂ showed a trap state energy level (E_a) at 0.27 eV, which was shallower than that of the control device (0.30 eV), meaning that some deep trap states were eliminated in the APDI₂-containing devices fabricated under the faster nucleation rate condition. It can be concluded that the THP colloidal solution with low absolute zeta potential improved the photovoltaic performance of tin halide-based PSCs.

Conclusion

In this work, we established a direct link between the zeta potential of the THP colloidal particles and the crystallization kinetics of THP films. The addition of APDI₂ into the pristine perovskite precursor solution led to zeta potential change from -4.22 mV to 0.69 mV . This change could be attributed to the strong chemisorption of APDI₂²⁺ into the Stern layer of the FASnI₃ colloids. The lower absolute value of the zeta potential for colloids with APDI₂ (0.69 mV) than that of the pristine colloids (4.22 mV) reduced the total interaction potential energy (E_p) between colloidal particles and the critical nucleation concentration (c_{\min}), which accelerated the nucleation rate. Laser light scattering measurement during spin-coating confirmed that the colloids modified by APDI₂ with lower absolute zeta potential had a faster nucleation rate, providing the advantages of fabricating full-coverage, high crystalline, and dense THP films with fewer defects. This innovation has allowed to achieve a PCE as high as 15.13% with decreased trap-assisted recombination and improved V_{oc} . Our study handpicks and draws on the fundamental colloidal property of zeta potential in the THP precursor solution, and provides a new method for accurately controlling the nucleation dynamics of THP films, thus clearing the colloidal chemistry path to engineering nontoxic lead-free perovskite solar cells.

Acknowledgements

This work was supported by the National Natural Science Foundation of China (22179131, U2001217, 22261160370, 22025208), the Fundamental Research Funds for the Central Universities, the University of Chinese Academy of Sciences, and Shenzhen Peacock Plan (KQTD2016053015544057). A portion of this work is based on the data obtained at BSRF-1W1A. The authors gratefully acknowledge the cooperation of the beamline scientists at BSRF-1W1A beamline.

Conflict of Interest

The authors declare no competing financial interest.

Data Availability Statement

The data that support the findings of this study are available from the corresponding author upon reasonable request.

Keywords: zeta potential · crystallization kinetics · lead-free · tin halide perovskite · solar cell

- [1] J. Park, J. Kim, H. S. Yun, M. J. Paik, E. Noh, H. J. Mun, M. G. Kim, T. J. Shin, S. I. Seok, *Nature* **2023**, *616*, 724–730.
- [2] M. M. Lee, J. Teuscher, T. Miyasaka, T. N. Murakami, H. J. Snaith, *Science* **2012**, *338*, 643–647.
- [3] Y. Fan, H. Chen, X. Liu, M. Ren, Y. Liang, Y. Wang, Y. Miao, Y. Chen, Y. Zhao, *J. Am. Chem. Soc.* **2023**, *145*, 8209–8217.
- [4] National Renewable Energy Laboratory. *Best Research-Cell Efficiencies*. <https://www.nrel.gov/pv/assets/pdfs/best-research-cell-efficiencies.pdf>. (date of access 25/10/2023).
- [5] W. Feng, J. Tao, G. Liu, G. Yang, J. X. Zhong, Y. Fang, L. Gong, S. Yang, W. Q. Wu, *Angew. Chem. Int. Ed.* **2023**, *62*, e202300265.
- [6] M. Wu, H. Wang, Y. Li, R. Chen, H. Zhou, S. Yang, D. Xu, K. Li, Z. An, S. F. Liu, Z. Liu, *Angew. Chem. Int. Ed.* **2023**, e202313472.
- [7] W. Ke, M. G. Kanatzidis, *Nat. Commun.* **2019**, *10*, 965.
- [8] L. Xu, X. Feng, W. Jia, W. Lv, A. Mei, Y. Zhou, Q. Zhang, R. Chen, W. Huang, *Energy Environ. Sci.* **2021**, *14*, 4292–4317.
- [9] M. Pitaro, E. K. Tekelenburg, S. Shao, M. A. Loi, *Adv. Mater.* **2022**, *34*, e2105844.
- [10] C. Ran, W. Gao, J. Li, J. Xi, L. Li, J. Dai, Y. Yang, X. Gao, H. Dong, B. Jiao, I. Spanopoulos, C. D. Malliakas, X. Hou, M. G. Kanatzidis, Z. Wu, *Joule* **2019**, *3*, 3072–3087.
- [11] Q. Tai, X. Guo, G. Tang, P. You, T. W. Ng, D. Shen, J. Cao, C. K. Liu, N. Wang, Y. Zhu, C. S. Lee, F. Yan, *Angew. Chem. Int. Ed.* **2019**, *58*, 806–810.
- [12] H. H. Fang, S. Adjokatsse, S. Shao, J. Even, M. A. Loi, *Nat. Commun.* **2018**, *9*, 243.
- [13] L. Wang, Q. Miao, D. Wang, M. Chen, H. Bi, J. Liu, A. K. Baranwal, G. Kapil, Y. Sanehira, T. Kitamura, T. Ma, Z. Zhang, Q. Shen, S. Hayase, *Angew. Chem. Int. Ed.* **2023**, *62*, e202307228.
- [14] C. Duan, F. Zou, Q. Wen, M. Qin, J. Li, C. Chen, X. Lu, L. Ding, K. Yan, *Adv. Mater.* **2023**, *35*, e2300503.
- [15] J. Liu, H. Yao, S. Wang, C. Wu, L. Ding, F. Hao, *Adv. Energy Mater.* **2023**, *13*, 2300696.
- [16] J. Zhao, Z. Zhang, G. Li, M. H. Aldamasy, M. Li, A. Abate, *Adv. Energy Mater.* **2023**, *13*, 2204233.
- [17] B. Chang, H. Li, L. Wang, L. Pan, Y. Wu, Z. Liu, L. Yin, *Adv. Funct. Mater.* **2023**, 2305852.
- [18] T. Li, Z. Zhang, F. He, L. Deng, Y. Yang, X. Mo, Y. Zhan, J. Liang, *Adv. Funct. Mater.* **2023**, 2308457.
- [19] H. Rao, Y. Su, G. Liu, H. Zhou, J. Yang, W. Sheng, Y. Zhong, L. Tan, Y. Chen, *Angew. Chem. Int. Ed.* **2023**, *62*, e202306712.
- [20] T. Li, F. He, J. Liang, Y. Qi, *Joule* **2023**, *7*, 1966–1991.
- [21] G. Liu, X. Jiang, W. Feng, G. Yang, X. Chen, Z. Ning, W. Q. Wu, *Angew. Chem. Int. Ed.* **2023**, e202305551.
- [22] J. Pascual, M. Flatken, R. Félix, G. Li, S. H. Turren-Cruz, M. H. Aldamasy, C. Hartmann, M. Li, D. Di Girolamo, G. Nasti, E. Hüsam, R. G. Wilks, A. Dallmann, M. Bär, A. Hoell, A. Abate, *Angew. Chem. Int. Ed.* **2021**, *60*, 21583–21591.
- [23] B. Li, C. Zhang, D. Gao, X. Sun, S. Zhang, Z. Li, J. Gong, S. Li, Z. Zhu, *Adv. Mater.* **2023**, e2309768.
- [24] Y. Gao, Z. Wei, P. Yoo, E. Shi, M. Zeller, C. Zhu, P. Liao, L. Dou, *J. Am. Chem. Soc.* **2019**, *141*, 15577–15585.
- [25] X. Qiu, J. Xia, Y. Liu, P. A. Chen, L. Huang, H. Wei, J. Ding, Z. Gong, X. Zeng, C. Peng, C. Chen, X. Wang, L. Jiang, L. Liao, Y. Hu, *Adv. Mater.* **2023**, e2305648.
- [26] H. Zhu, W. Yang, Y. Reo, G. Zheng, S. Bai, A. Liu, Y.-Y. Noh, *Nature Electronics* **2023**, *6*, 650–657.
- [27] D. Han, J. Wang, L. Agosta, Z. Zang, B. Zhao, L. Kong, H. Lu, I. Mosquera-Lois, V. Carnevali, J. Dong, J. Zhou, H. Ji, L. Pfeifer, S. M. Zakeeruddin, Y. Yang, B. Wu, U. Rothlisberger, X. Yang, M. Gratzel, N. Wang, *Nature* **2023**, doi: 10.1038/s41586-41023-06514-41586.
- [28] H. Min, J. Chang, Y. Tong, J. Wang, F. Zhang, Z. Feng, X. Bi, N. Chen, Z. Kuang, S. Wang, L. Yuan, H. Shi, N. Zhao, D. Qian, S. Xu, L. Zhu, N. Wang, W. Huang, J. Wang, *Nat. Photonics* **2023**, *17*, 755–760.
- [29] C. K. Liu, Q. Tai, N. Wang, G. Tang, H. L. Loi, F. Yan, *Adv. Sci.* **2019**, *6*, 1900751.
- [30] G. Xing, M. H. Kumar, W. K. Chong, X. Liu, Y. Cai, H. Ding, M. Asta, M. Gratzel, S. Mhaisalkar, N. Mathews, T. C. Sum, *Adv. Mater.* **2016**, *28*, 8191–8196.
- [31] J. Zhou, M. Hao, Y. Zhang, X. Ma, J. Dong, F. Lu, J. Wang, N. Wang, Y. Zhou, *Matter* **2022**, *5*, 683–693.
- [32] X. Jiang, H. Li, Q. Zhou, Q. Wei, M. Wei, L. Jiang, Z. Wang, Z. Peng, F. Wang, Z. Zang, K. Xu, Y. Hou, S. Teale, W. Zhou, R. Si, X. Gao, E. H. Sargent, Z. Ning, *J. Am. Chem. Soc.* **2021**, *143*, 10970–10976.
- [33] L. Mao, C. C. Stoumpos, M. G. Kanatzidis, *J. Am. Chem. Soc.* **2019**, *141*, 1171–1190.
- [34] B. B. Yu, Z. Chen, Y. Zhu, Y. Wang, B. Han, G. Chen, X. Zhang, Z. Du, Z. He, *Adv. Mater.* **2021**, *33*, 2102055.
- [35] C. H. Kuan, R. Balasaravanan, S. M. Hsu, J. S. Ni, Y. T. Tsai, Z. X. Zhang, M. C. Chen, E. W. Diau, *Adv. Mater.* **2023**, *35*, e2300681.
- [36] K. O. Ighodalo, W. Chen, Z. Liang, Y. Shi, S. Chu, Y. Zhang, R. Khan, H. Zhou, X. Pan, J. Ye, Z. Xiao, *Angew. Chem. Int. Ed.* **2023**, *62*, e202213932.
- [37] J. Cao, F. Yan, *Energy Environ. Sci.* **2021**, *14*, 1286–1325.
- [38] L. Zhu, H. Cao, C. Xue, H. Zhang, M. Qin, J. Wang, K. Wen, Z. Fu, T. Jiang, L. Xu, Y. Zhang, Y. Cao, C. Tu, J. Zhang, D. Liu, G. Zhang, D. Kong, N. Fan, G. Li, C. Yi, Q. Peng, J. Chang, X. Lu, N. Wang, W. Huang, J. Wang, *Nat. Commun.* **2021**, *12*, 5081.
- [39] S. Zou, S. Ren, Y. Jiang, Y. Huang, W. Wang, C. Wang, C. Chen, X. Hao, L. Wu, J. Zhang, D. Zhao, *Energy Environ. Sci.* **2023**, doi: 10.1002/eeem1002.12465.
- [40] R. Munir, A. D. Sheikh, M. Abdelsamie, H. Hu, L. Yu, K. Zhao, T. Kim, O. E. Tall, R. Li, D. M. Smilgies, A. Amassian, *Adv. Mater.* **2017**, *29*, 1604113.

- [41] X. Du, J. Zhang, H. Su, X. Guo, Y. Hu, D. Liu, N. Yuan, J. Ding, L. Gao, S. F. Liu, *Adv. Mater.* **2022**, *34*, e2204098.
- [42] Z. Xing, X. Meng, D. Li, T. Hu, X. Hu, Y. Chen, *Sci Bull (Beijing)* **2022**, *67*, 561–564.
- [43] K. Yan, M. Long, T. Zhang, Z. Wei, H. Chen, S. Yang, J. Xu, *J. Am. Chem. Soc.* **2015**, *137*, 4460–4468.
- [44] D. P. McMeekin, Z. Wang, W. Rehman, F. Pulvirenti, J. B. Patel, N. K. Noel, M. B. Johnston, S. R. Marder, L. M. Herz, H. J. Snaith, *Adv. Mater.* **2017**, *29*, 1607039.
- [45] J. Kim, B. W. Park, J. Baek, J. S. Yun, H. W. Kwon, J. Seidel, H. Min, S. Coelho, S. Lim, S. Huang, K. Gaus, M. A. Green, T. J. Shin, A. W. Y. Ho-Baillie, M. G. Kim, S. I. Seok, *J. Am. Chem. Soc.* **2020**, *142*, 6251–6260.
- [46] X. Meng, Y. Li, Y. Qu, H. Chen, N. Jiang, M. Li, D. J. Xue, J. S. Hu, H. Huang, S. Yang, *Angew. Chem. Int. Ed.* **2021**, *60*, 3693–3698.
- [47] B. Zhao, S. F. Jin, S. Huang, N. Liu, J. Y. Ma, D. J. Xue, Q. Han, J. Ding, Q. Q. Ge, Y. Feng, J. S. Hu, *J. Am. Chem. Soc.* **2018**, *140*, 11716–11725.
- [48] X. Xiao, W. Zhang, W. Zhang, J. Du, C. Zhang, G. Xu, A. Mei, Y. Rong, Y. Hu, H. Han, *Chem. Mater.* **2022**, *34*, 2231–2237.
- [49] D. Bi, C. Yi, J. Luo, J.-D. Décoppet, F. Zhang, Shaik M. Zakeeruddin, X. Li, A. Hagfeldt, M. Grätzel, *Nat. Energy* **2016**, *1*, 16142.
- [50] Y. Zou, P. Teng, W. Xu, G. Zheng, W. Lin, J. Yin, L. Kobera, S. Abbrent, X. Li, J. A. Steele, E. Solano, M. B. J. Roeffaers, J. Li, L. Cai, C. Kuang, I. G. Scheblykin, J. Brus, K. Zheng, Y. Yang, O. F. Mohammed, O. M. Bakr, T. Pullerits, S. Bai, B. Sun, F. Gao, *Nat. Commun.* **2021**, *12*, 4831.
- [51] D. Zheng, F. Raffin, P. Volovitch, T. Pauporte, *Nat. Commun.* **2022**, *13*, 6655.
- [52] K. Agarwal, M. Trivedi, C. D. Ohl, N. Nirmalkar, *Langmuir* **2023**, *39*, 5250–5262.
- [53] X. Wang, K. Liu, J. Wu, *J. Chem. Phys.* **2021**, *154*, 124701.
- [54] J. P. Hsu, B. T. Liu, *J. Phys. Chem. B.* **1998**, *102*, 334–337.
- [55] J. Wu, *Chem. Rev.* **2022**, *122*, 10821–10859.
- [56] H. Ding, S. R. Rahman, *Energy Fuels* **2018**, *32*, 9314–9321.
- [57] T. L. Moore, L. Rodriguez-Lorenzo, V. Hirsch, S. Balog, D. Urban, C. Jud, B. Rothen-Rutishauser, M. Lattuada, A. Petri-Fink, *Chem. Soc. Rev.* **2015**, *44*, 6287–6305.
- [58] J. P. Hsu, H. Y. Yu, S. Tseng, *J. Phys. Chem. B* **2006**, *110*, 7600–7604.
- [59] J. P. Hsu, S. H. Lin, S. J. Tseng, *J. Phys. Chem. B.* **2004**, *108*, 4495–4500.
- [60] M. Jung, S. G. Ji, G. Kim, S. I. Seok, *Chem. Soc. Rev.* **2019**, *48*, 2011–2038.
- [61] M. Cerdeira, R. J. Candal, M. L. Herrera, *J. Food Sci.* **2006**, *69*, 185–191.
- [62] S. Cherthazhekatt, D. D. Robertson, M. Brand, A. van Reenen, H. Pasch, *Anal. Chem.* **2013**, *85*, 7019–7023.
- [63] A. van Reenen, M. Brand, E. Rohwer, P. Walters, *Macro. Symp.* **2009**, *282*, 25–32.
- [64] Q. Cheng, B. Wang, G. Huang, Y. Li, X. Li, J. Chen, S. Yue, K. Li, H. Zhang, Y. Zhang, H. Zhou, *Angew. Chem. Int. Ed.* **2022**, *61*, e202208264.
- [65] J. Wang, C. Yang, H. Chen, M. Lv, T. Liu, H. Chen, D.-J. Xue, J.-S. Hu, L. Han, S. Yang, X. Meng, *ACS Energy Lett.* **2023**, *8*, 1590–1596.
- [66] X. Jiang, F. Wang, Q. Wei, H. Li, Y. Shang, W. Zhou, C. Wang, P. Cheng, Q. Chen, L. Chen, Z. Ning, *Nat. Commun.* **2020**, *11*, 1245.

Manuscript received: November 21, 2023

Accepted manuscript online: February 29, 2024

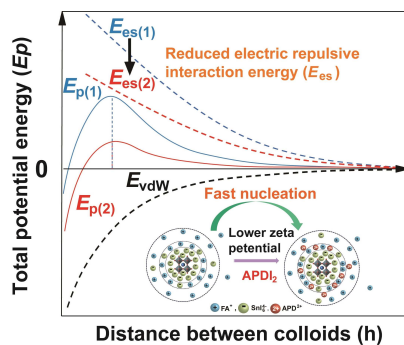
Version of record online: ■■■, ■■■

Forschungsartikel

Solar Cells

J. Wang, J. Huang, M. Abdel-Shakour, T. Liu, X. Wang, Y. Pan, L. Wang, E. Cui, J.-S. Hu,* S. Yang,* X. Meng* — e202317794

Colloidal Zeta Potential Modulation as a Handle to Control the Crystallization Kinetics of Tin Halide Perovskites for Photovoltaic Applications



We provided a new method for accurately controlling the nucleation kinetics of tin halide perovskite films through modulating zeta potential of tin halide perovskite colloids. A fast nucleation rate was achieved by adding 3-amino-pyrrolidine dihydroiodate (APDI₂) in the precursor solution to change the zeta potential of the FASnI₃ colloids. The high-quality tin halide perovskite film with APDI₂ yields a high photovoltaic efficiency of 15.13%.